

SCIENTIFIC REPORTS

OPEN

Prostaglandin E₂ glyceryl ester is an endogenous agonist of the nucleotide receptor P2Y₆

Antje Brüser¹, Anne Zimmermann¹, Brenda C. Crews², Gregory Sliwoski⁵, Jens Meiler³, Gabriele M. König⁴, Evi Kostenis⁴, Vera Lede¹, Lawrence J. Marnett² & Torsten Schöneberg¹

Cyclooxygenase-2 catalyses the biosynthesis of prostaglandins from arachidonic acid but also the biosynthesis of prostaglandin glycerol esters (PG-Gs) from 2-arachidonoylglycerol. Previous studies identified PG-Gs as signalling molecules involved in inflammation. Thus, the glyceryl ester of prostaglandin E₂, PGE₂-G, mobilizes Ca²⁺ and activates protein kinase C and ERK, suggesting the involvement of a G protein-coupled receptor (GPCR). To identify the endogenous receptor for PGE₂-G, we performed a subtractive screening approach where mRNA from PGE₂-G response-positive and -negative cell lines was subjected to transcriptome-wide RNA sequencing analysis. We found several GPCRs that are only expressed in the PGE₂-G responder cell lines. Using a set of functional readouts in heterologous and endogenous expression systems, we identified the UDP receptor P2Y₆ as the specific target of PGE₂-G. We show that PGE₂-G and UDP are both agonists at P2Y₆, but they activate the receptor with extremely different EC₅₀ values of ~1 pM and ~50 nM, respectively. The identification of the PGE₂-G/P2Y₆ pair uncovers the signalling mode of PG-Gs as previously under-appreciated products of cyclooxygenase-2.

Prostaglandins are potent bioactive lipid messengers derived from arachidonic acid¹. Cyclooxygenases (COXs) catalyse the rate-limiting step of prostaglandin biosynthesis. Besides this well-studied enzymatic function of COX isoenzymes, COX-2 selectively oxygenates 2-arachidonoylglycerol (2-AG) to form prostaglandin glycerol esters (PG-Gs)². The initially formed PG-G endoperoxides are further transformed to PGE₂-G, PGD₂-G, PGF_{2α}-G, and PGI₂-G³. Despite its rapid degradation⁴, PGE₂-G is detectable following activation of different macrophage cell lines^{5–8} and is present in rat paw after treatment with carrageenan⁹. This implicates PG-Gs as potential mediators of pain and the innate immune response.

Very little is known about the biological function of PG-Gs. PGE₂-G induces hyperalgesia⁹, improves excitatory glutamatergic synaptic transmission, and promotes neurotoxicity in rat hippocampal neurons¹⁰. Previous work suggests that PGE₂-G activates a G protein-coupled receptor (GPCR) in the murine macrophage-like cell line RAW264.7 and the human lung adenocarcinoma cell line H1819^{11,12}. The fast Ca²⁺ response observed with both cell lines indicates specific signal transduction via a G_q- and/or G_i protein-coupled receptor. Interestingly, these studies revealed an extremely low EC₅₀ value in the range of 1 pM for PGE₂-G. Physiologically, this seems reasonable because PGE₂-G occurs in low amounts and is rapidly hydrolysed to PGE₂⁴. Indeed, stimulation of macrophages with lipopolysaccharide and zymosan induces synthesis of PGE₂-G in amounts sufficient to activate the unknown PGE₂-G receptor⁷.

Identification of the PGE₂-G receptor is of great interest as a first step toward characterizing the physiological function of PG-Gs and to pharmacologically manipulate this signalling system. Since previous attempts demonstrated that PGE₂-G does not efficiently activate the known prostanoid receptors EP_{1–4}, DP, FP, TP, or IP^{9,11,13}, we extended our search by screening all currently known orphan GPCRs for PGE₂-G activation. However, this

¹Rudolf Schönheimer Institute of Biochemistry, Medical Faculty, University of Leipzig, 04103, Leipzig, Germany.

²Department of Biochemistry, Chemistry and Pharmacology, Vanderbilt Institute of Chemical Biology, Vanderbilt-Ingram Cancer Center, Vanderbilt University School of Medicine, Nashville, TN, 37232-0146, USA. ³Department of Chemistry, Center for Structural Biology, Vanderbilt University, Nashville, TN, 37232-8725, USA. ⁴Institute of Pharmaceutical Biology, University of Bonn, 53115, Bonn, Germany. ⁵Department of Biomedical Informatics, Vanderbilt University School of Medicine, Nashville, TN, 37232-8725, USA. Antje Brüser and Anne Zimmermann contributed equally to this work. Correspondence and requests for materials should be addressed to A.B. (email: antje.brueser@medizin.uni-leipzig.de) or T.S. (email: schoberg@medizin.uni-leipzig.de)

classical approach to identify the endogenous receptor for PGE₂-G was unsuccessful. Therefore, we sequenced the transcriptome of several PGE₂-G responder and non-responder cell lines using Illumina RNA sequencing technology. In a subtractive approach, we identified several GPCRs, which are significantly expressed in the PGE₂-G responder cell lines. Cloning and functional testing of these receptors were performed and revealed the UDP receptor P2Y₆ as the GPCR for PGE₂-G.

Results

Screening of orphan GPCRs. Because previous studies failed to show binding or activation of PGE₂-G at the known prostanoid receptors^{9,11,13}, we attempted to identify a receptor among GPCRs which were considered orphan at this time. In a Path-Hunter[®] biosensor Orphan GPCR cell line panel (DiscoverRx, USA), 78 orphan GPCRs were tested for their ability to be activated by PGE₂-G. None of the tested receptors demonstrated a positive response (Supplementary Table S1).

RNA sequencing reveals differentially expressed G_q/G_i protein-coupled receptors in PGE₂-G-responding cell lines. As seen in Fig. 1a, a Ca²⁺ mobilization assay confirms previous findings that PGE₂-G activates its putative receptor in H1819 and RAW264.7 cells with EC₅₀ values of 0.7 pM and 0.8 pM, respectively^{11,12}. PGE₂-G had no effect on HEK293 cells. This led to the hypothesis that subtraction of all GPCRs expressed in both, PGE₂-G-responding and -non-responding cells would provide a set of receptors that are found only in the PGE₂-G-responder cell lines. Thus, mRNA was extracted from these cell lines and the additional PGE₂-G-non-responding cell lines cell lines, A7r5 and A431¹¹. The mRNA was subjected to RNA sequencing. The analysis revealed that a broad range of GPCRs is expressed in these cell lines (Supplementary Table S2). The number of expressed receptors above a threshold of FPKM value >1 (FPKM, fragments per kilobase of transcript per million mapped reads) was 65 (RAW264.7), 71 (A7r5), 108 (HEK293), 83 (A431), and 52 (H1819). Only 6 receptors were expressed exclusively in the PGE₂-G-responding cell lines H1819 and RAW264.7 (Table 1, Fig. 1b). All 6 receptors are non-orphan GPCRs. GPR183, also known as the Epstein-Barr virus-induced receptor 2 (EBI2), is activated by 7 α ,25-dihydroxycholesterol and couples to G_{i/o} proteins^{14–16}. The chemokine (C-C-motif) receptor 10 (CCR10) is activated by the chemokines CCL27 and CCL28¹⁷. GPR68 is known as a pH-sensing receptor and is involved in regulation of IL6-production¹⁸, and GPR132 can be activated by commendamide¹⁹. UDP is the agonist of P2Y₆ and activation of P2Y₆ results in generation of inositol-1,4,5-trisphosphate (IP₃) and the subsequent release of intracellular Ca²⁺^{20,21}. Further, G_i protein-coupling was described for P2Y₆²². 2-AG is the agonist of cannabinoid receptor 2 (Cnr2)²³.

To further prioritize the list of GPCRs for testing, we compared the expression levels (read counts) of the 6 GPCRs between the human responder and non-responder cell lines (Table 1). Only the UDP receptor P2Y₆ showed significantly higher expression levels in the responder cell line H1819 compared to HEK293 and A431 ($p = 0.005$). Since our previous findings suggested that the putative PGE₂-G receptor signals via a G_q and/or G_{i/o} protein^{11,12} we focused on P2Y₆ for further analyses.

UDP and PGE₂-G elevate cytosolic Ca²⁺ levels in RAW264.7 and H1819 cells. First, to validate the RNA sequencing result that P2Y₆ is expressed in H1819 and RAW264.7 cells, we immunologically determined the receptor expression at the plasma membrane with a cell surface ELISA and measured intracellular Ca²⁺ release upon UDP stimulation. As shown in Fig. 1c, P2Y₆ is endogenously expressed in H1819 and RAW264.7 cells but not in PGE₂-G response-negative HEK293 cells. Further, UDP is an agonist in the Ca²⁺ assay with EC₅₀ values of 38.4 ± 1.9 and 25.9 ± 2.8 nM in RAW264.7 and H1819 cells, respectively, and has no effect on HEK293 cells (Fig. 1d). The EC₅₀ values were almost identical to the EC₅₀ value determined in 1321N1 human astrocytoma cells stably transfected with P2RY6²⁴.

Next, we cloned the human P2RY6 into the mammalian expression vector pcDps to test the ability of PGE₂-G to activate this receptor in a heterologous expression system. After transfection, the receptor was detectable at the surface of HEK293 cells (Fig. 2a). Both, PGE₂-G and UDP increased the cytosolic Ca²⁺ levels in HEK293 cells transiently transfected with P2RY6 in a concentration-dependent manner (Fig. 2b) whereas PGE₂-G and UDP had no effect on non-transfected cells (Fig. 1a and d). PGE₂-G revealed the same potency (~1 pM) as observed in RAW264.7 and H1819 cells^{11,12}. Because Cnr2 is exclusively expressed in PGE₂-G-responding cells (Table 1), and its agonist 2-AG is chemically related to PGE₂-G, we transiently transfected CNR2 in HEK293 cells for functional testing. 2-AG induced a robust intracellular Ca²⁺ increase in these cells, but PGE₂-G did not (Fig. 2c), excluding this receptor as potential target of PGE₂-G.

UDP- and PGE₂-G-activated P2Y₆ couples to G_q- and G_{i/o} proteins. As previously shown, PGE₂-G induces an increase in IP₃ levels in RAW264.7 cells¹¹. We performed an IP₃ assay in P2RY6-transfected HEK293 cells. Stimulation with UDP and PGE₂-G increased IP₃ levels with EC₅₀ values of 2.7 ± 0.1 nM and 0.2 ± 0.01 pM, respectively, (Fig. 3a). In addition, activation by UDP and PGE₂-G led to ERK1/2 phosphorylation (Fig. 3b) in P2RY6-transfected HEK293 cells, and both compounds suppressed cAMP formation in these cells with EC₅₀ values of 0.6 ± 0.2 pM and 3.6 ± 0.3 nM for PGE₂-G and UDP, respectively (Fig. 3c). The specificity of G_q coupling after PGE₂-G activation was verified with a selective inhibitor for the G_q protein²⁵ (UBO). UBO can significantly block the IP formation after stimulation with UDP and PGE₂-G (Fig. 3d).

In previous studies, Nirodi and co-workers showed that PGF_{2 α} led to Ca²⁺ release in RAW264.7 cells¹¹. To provide evidence that the PGF_{2 α} response is not caused by P2Y₆, we tested PGF_{2 α} on HEK293 cells transfected with P2RY6. As shown in Fig. 3e, PGF_{2 α} had no effect on these cells. Additionally, PGF_{2 α} -G, and PGE₂ showed no response in P2RY6-transfected cells (Fig. 3e). These results are consistent with previous observation that PGD₂-G, PGF_{2 α} -G, and PGE₂ had no effect on RAW264.7 cells in Ca²⁺ measurements¹¹. Finally, to test whether PGE₂-G activates other P2Y receptors, we tested P2Y₁ and P2Y₁₂ for Ca²⁺ release upon PGE₂-G stimulation. As shown

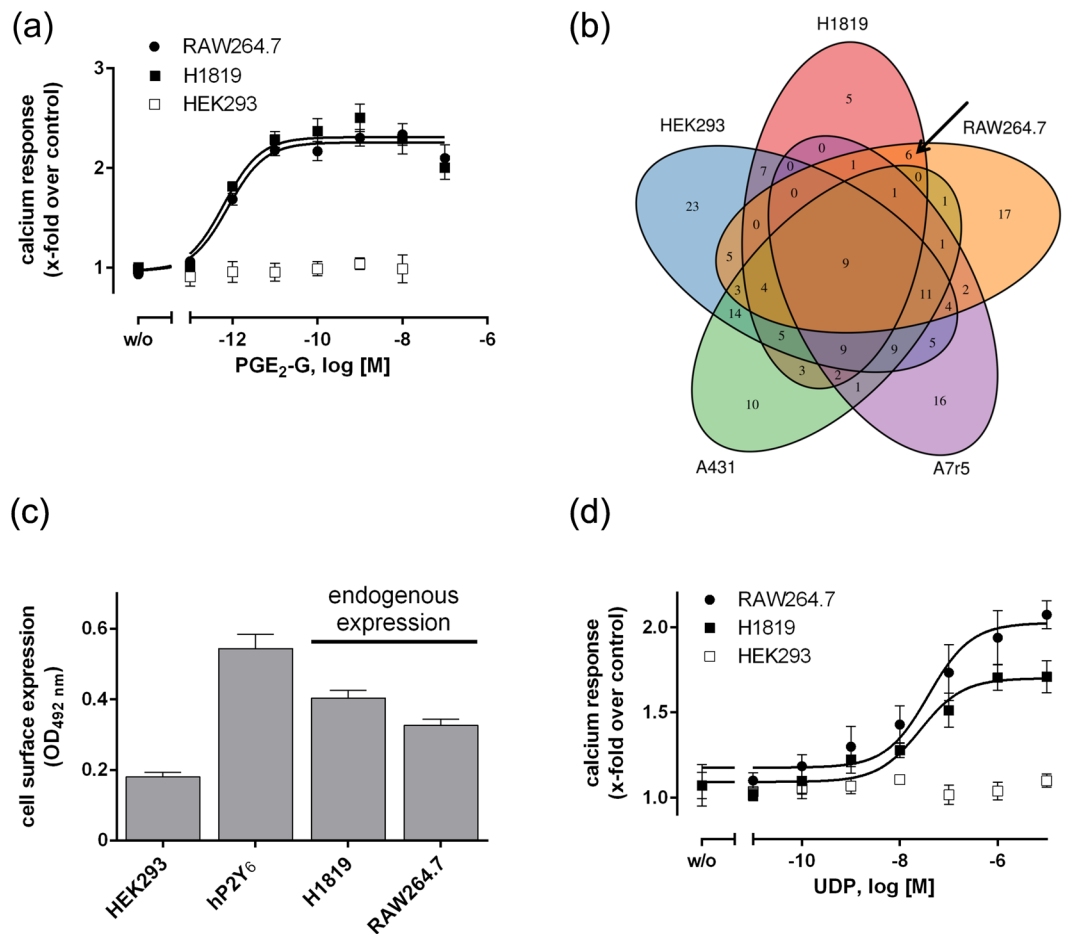


Figure 1. PGE₂-G induces intracellular Ca²⁺ release in different cell lines. **(a)** Different cells lines were treated with the indicated concentrations of PGE₂-G, and intracellular Ca²⁺ measurement was performed as described (see Methods). EC₅₀ values were 0.8 ± 0.1 and 0.7 ± 0.1 pM for RAW264.7 and H1819 cell, respectively. Relative Fluorescence Units (RFU) for control (1% DMSO) were $1,560 \pm 479$, $2,106 \pm 1,193$, and $5,247 \pm 2,016$ for RAW264.7, HEK293, and H1819 cells, respectively. Maximum RFU for PGE₂-G were $3,649 \pm 678$, $2,193 \pm 252$ and $13,143 \pm 2,157$ for RAW264.7, HEK293, and H1819 cells, respectively. Data are shown as $RFU_{max} - RFU_{min}$ (ligand)/ $RFU_{max} - RFU_{min}$ (control). Data are means \pm SEM of three experiments, each performed in quadruplicate. **(b)** Expression of GPCRs in the investigated cell lines. The Venn-Diagram shows the number of expressed GPCRs in the investigated cell lines. Numbers in non-overlapping regions correspond to the number of GPCRs specific for the respective cell line, whereas numbers in the overlapping areas correspond to receptors shared by two or more cell lines. 6 GPCRs were exclusively expressed in the two PGE₂-G-responding cell lines (indicated by arrow). Receptors with an FPKM >1 were considered to be expressed. **(c)** Endogenous expression levels of P2Y₆ in H1819 and RAW264.7 cells were determined by a cell surface ELISA using an N-terminally directed anti P2Y₆ antibody (see Methods). HEK293 cells served as negative control and HEK293 cells stably transfected with hp2RY6 as positive control. Protein expression is given as optical density (OD). To determine unspecific antibody binding empty wells were treated similarly and revealed an OD_{492 nm} of 0.16 ± 0.04 . Data are given as means \pm SEM of three independent experiments each performed in quadruplicates. **(d)** The effect of UDP on intracellular Ca²⁺ release was measured in H1819 and RAW264.7 cells (see Methods). Cell lines were incubated with the indicated concentrations of UDP and EC₅₀ values were 38.4 ± 1.9 and 25.9 ± 2.8 nM for RAW264.7 and H1819 cells, respectively.

in Fig. 3f these receptors led to Ca²⁺ release after stimulation with their agonist ADP but not with PGE₂-G. This indicates that the PGE₂-G/P2Y₆ pair is a highly specific endogenous signalling system.

Next, we tested whether P2Y₆ activation is responsible for the previously reported PGE₂-G-induced ERK1/2 phosphorylation in RAW264.7 and H1819 cells^{11,12}. We performed siRNA knock-down experiments for the mouse and human P2RY6 orthologues in RAW264.7 and H1819 cells, respectively. Knock-down of the receptor mRNA and protein expression was verified by RT-qPCR experiments and cell surface ELISA, respectively. As shown in Fig. 4a,b, a significant down-regulation of P2RY6 mRNA and P2Y₆ protein expression was found after 48 h. The down-regulation also decreased ERK1/2 phosphorylation and Ca²⁺ release after stimulation with UDP and PGE₂-G (Fig. 4c-f).

name	gene.id (human)	FPKM					p-value
		A431	HEK293	A7r5	H1819	RAW264.7	
P2RY6	ENSG00000171631	0.18	0.29	0.9	10.09	46.64	0.005
CCR10	ENSG00000184451	0	0	0.55	7.68	3.15	0.09
CNR2	ENSG00000188822	0	0	0	1.67	2.48	0.11
GPR68	ENSG00000119714	0.51	0.36	0	1.8	9.76	0.63
GPR183	ENSG00000169508	0.14	0	0.13	1.74	39.58	1
GPR132	ENSG00000183484	0.35	0.99	0	1.55	5.69	1

Table 1. GPCRs significantly expressed only in the PGE₂-G-responding cell lines RAW264.7 and H1819. The p-value is from the differential expression analysis of the human cell lines (see *Methods*).

Increasing concentrations of the selective P2Y₆ antagonist MRS2578²⁶ reduced both the efficacies and potencies of UDP-induced IP₁ accumulation (Fig. 5a). The different MRS2578 concentrations had a similar effect on UDP- and PGE₂-G-triggered IP₁ accumulation (Fig. 5b). Similarly, MRS2578 had the same effects on UDP- and PGE₂-G-triggered Ca²⁺ release (Fig. 5c,d). Finally, we studied agonist-induced receptor internalization in the cell surface ELISA. As shown in Fig. 5e, cell surface expression levels of P2Y₆ were reduced following UDP and PGE₂-G stimulation and the time-dependent internalization showed no differences between the agonists. The antagonist MRS2578 blocked the internalization (Fig. 5e).

In sum these data clearly demonstrate that signal transduction of PGE₂-G requires the presence of the UDP receptor P2Y₆. Our results indicate that the antagonist MRS2578 has very similar effects on the function of both UDP and PGE₂-G. This is compatible with a scenario that both agonists share the binding side but it does not prove it. However, there is also the possibility that PGE₂-G somehow releases UDP from the cell which in an autocrine or paracrine manner activates P2Y₆. To convincingly demonstrate that PGE₂-G directly acts on P2Y₆, we explored the binding sites of both agonists. The identification of determinants that are specific for binding of only one of the agonists would be highly supportive for a two-agonists-scenario at P2Y₆.

UDP and PGE₂-G share the ligand binding site of P2Y₆. UDP is a well-established endogenous agonist for P2Y₆²¹. Our studies above showed that application of both, UDP and PGE₂-G, leads to activation of the human and mouse P2Y₆. This raises the question of whether the binding sites for UDP and PGE₂-G at P2Y₆ overlap or are separated from each other. Unfortunately, there is no competitive antagonist specific for UDP at P2Y₆ and, therefore, Schild plot analyses could not be properly performed to clearly answer this question. However, to experimentally approach this important question we incubated P2RY6-transfected HEK cells with a submaximal concentration of UDP and performed concentration-response curve of PGE₂-G in an IP₁ accumulation assays. As shown in Fig. 6a, UDP at non-saturating concentrations (50 nM) increased IP₁ formation. Addition of increasing concentrations of PGE₂-G further elevated IP₁ levels but did not change the maximum response in this assay in an additive manner. EC₅₀ values of UDP and PGE₂-G alone were 77.3 ± 3.4 nM and 0.3 ± 0.02 pM, respectively (Fig. 6a). In the presence of sub-maximum UDP concentration the concentration-response curve of PGE₂-G shifted to higher concentrations with an EC₅₀ of 27.6 ± 2.8 pM. This result is difficult to interpret because it does not exclude different binding sides but it also does not directly support it (see *Discussion*).

Currently, there is no direct structural information on the P2Y₆. However, recent advances in solving the crystal structures of other GPCRs allow for generation of a P2Y₆ homology model and ligand docking. To estimate whether the different agonists may have similar binding properties, we simulated binding by docking the agonists into the comparative model of P2Y₆ (Fig. 6b). The model suggested that UDP and PGE₂-G have an overlapping binding pocket bordered by transmembrane helices (TM) 3, 6, and 7 with PGE₂-G extending further to TM 2. The model suggests that UDP and PGE₂-G share a number of interaction determinants but some are specific for the individual agonists. For example, UDP has distinct interactions with position R287 and Y262 whereas PGE₂-G is orientated to position Y75, R287 and F252.

To study the functional relevance of the individual positions we performed mutagenesis studies, changing the positions individually to alanine and testing the mutants in IP₁ accumulation assays. All mutants were expressed at the cell surface (Fig. 6c). Mutation of position Y262 to alanine displayed significantly reduced activity upon stimulation with UDP but was fully activated by PGE₂-G (Fig. 6d). Alanine mutation of the positions Y75 and F252, predicted to interact only with PGE₂-G, resulted in a loss of PGE₂-G-induced IP₁ formation, whereas UDP efficacy remained unchanged. Finally, alanine substitution of position R287 decreased receptor function for both agonists (Fig. 6d). In concentration-response experiments UDP displayed unchanged EC₅₀ values at mutant receptors Y75A and F252A with 15.4 ± 0.9 nM and 12.7 ± 2.1 nM, respectively (Fig. 6e). The ability to separate the activation abilities of UDP and PGE₂-G by distinct mutations excludes the possibility that a PGE₂-G-induced UDP release and subsequent P2Y₆ activation is responsible for the activity of PGE₂-G at P2Y₆-expressing cells.

Discussion

Prostaglandin glycerol esters represent a separate class of prostaglandins that derive from COX-2-selective oxygenation of 2-AG. In contrast to prostaglandins, which have been extensively studied for physiological functions and receptor signalling, the function and signalling pathway(s) of PG-Gs are still unknown. Here, we describe P2Y₆ as a physiological target of this unique group of bioactive lipids. After transient and stable expression in HEK293 cells and testing in different functional assays (see Figs 2–6) P2Y₆ was discovered to be

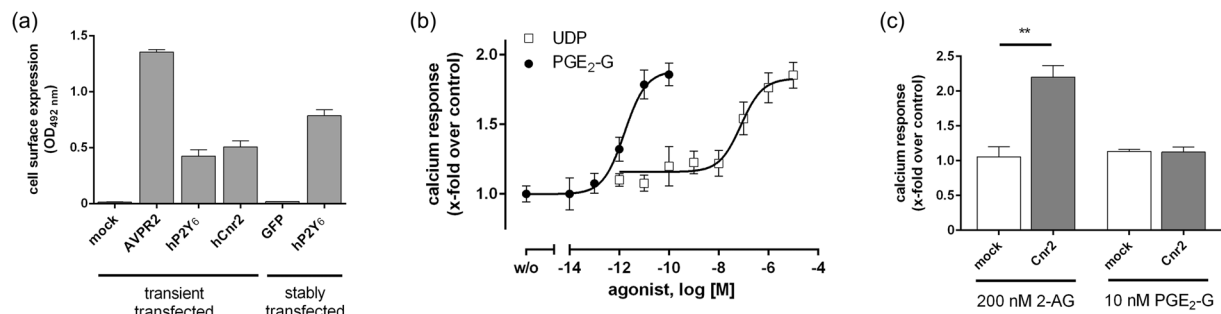


Figure 2. Effect of UDP and PGE₂-G on transfected HEK293 cells. **(a)** HEK293 cells were transiently transfected with either HA-tagged version of hP2RY6 and hCNR2 and the expression levels of receptors were measured by a cell surface ELISA (see *Methods*). As a positive control the human V2-vasopressin receptor (hAVPR2), N-terminally tagged with an HA tag, was used. eGFP and hP2RY6_eGFP were stably transfected in HEK293 cells and cell surface expression was measured. **(b)** HEK293 cells transfected with P2RY6 were used for intracellular Ca²⁺ measurements (see *Methods*). Indicated concentrations of UDP and PGE₂-G revealed EC₅₀ values of 78.3 ± 6.7 nM and 1.2 ± 0.08 pM, respectively. **(c)** In contrast to PGE₂-G, 200 nM of 2-AG elevated intracellular Ca²⁺ in CNR2-transfected cells. RFU for mock-transfected cells were 1,832 ± 299. All data are given as means ± SEM of three independent experiments each performed in triplicate. *p < 0.05, **p < 0.01, ***p < 0.001 (paired Student's t test).

the G_i/G_q protein-coupled receptor for PGE₂-G. Activation of this signalling pathway resulted in reduction of intracellular cAMP levels, ERK1/2 phosphorylation, IP formation, and intracellular Ca²⁺ release similar to those found in a macrophage cell line RAW264.7 and H1819 cells (see Fig. 1a) where P2Y₆ is highly expressed (Table 1; Fig. 1c).

Classically, agonist/GPCR pairs have been identified by screening potential targets (e.g., GPCR libraries) with a biologically active compound and iterative enrichment of mRNA from cells/organs that respond to this compound. The “reverse pharmacology” approach starts with tissue extracts that have an effect on a given target, e.g., an orphan GPCR. Using different purification and fractionation steps, the endogenous agonist can be identified within those extracts²⁷. Here, we took advantage of next generation sequencing technology to compare the transcriptomes of PGE₂-G-responding and non-responding cell lines in a subtractive approach. We used this approach not only to identify the receptors existing in PGE₂-G-responding cells but also to provide specific controls. For example, PGE₂-G is highly specific at P2Y₆ because other structurally related GPCRs of the P2Y group with similar signal transduction abilities were either tested in the orphan GPCR-expressing cell line panel (see Supplementary Table S1) or were not exclusively expressed in PGE₂-G responding cell lines (see Supplementary Table S3). Additionally, other P2Y receptors do not increase intracellular Ca²⁺ levels upon PGE₂-G stimulation in a heterologous expression system (see Fig. 3f).

P2Y₆ is expressed in a number of cells and tissues including the spleen, thymus, intestine, leukocytes, and aorta. Studies with P2Y₆-deficient mice have shown that this receptor is involved in both, the direct contraction and endothelium-dependent relaxation of the aorta by UDP²⁸. Its relevance in immune functions was demonstrated in P2Y₆-deficient CD4⁺ T cells where the receptor fine-tunes the activation of T cells in allergen-induced pulmonary inflammation^{29,30}. Further, P2Y₆ deficiency can reduce macrophage-mediated cholesterol uptake in atherosclerotic lesions³¹. One can speculate that, besides UDP, PGE₂-G is involved in mediating these functions. However, dissecting PGE₂-G-mediated effects from those of UDP is not trivial since specific inhibition of PGE₂-G biosynthesis is currently not possible and COX-2 inhibition will always affect other prostaglandins and PG-Gs. Therefore, development of PGE₂-G-specific receptor blockers or synthesis of inhibitors is required to identify the physiological contributions of PGE₂-G and UDP to P2Y₆-mediated signalling.

The endogenous agonists for most GPCRs have EC₅₀ values > 1 nM but rarely below 10 pM. With an EC₅₀ value of ~1 pM the PGE₂-G/P2Y₆ is an extraordinarily high affinity agonist/receptor pair. This is consistent with the observation that PGE₂-G is synthesized in low concentrations by COX-2 in macrophages and is susceptible to hydrolysis^{4,7}. Activation of P2Y₆ would require high affinity to meet these physiological conditions. The inducible enzyme COX-2 is expressed in neurons and radial glia cells and is involved in pathophysiological responses such as inflammation and allergic responses³². A recent study revealed a role of COX-2-derived PGE₂-G in inflammation and macrophage activation, further increasing IL-1β production and hyperalgesia⁵. Additionally, PGE₂-G influences pain sensitivity⁹ and is involved in lowering intraocular pressure³³. These observations suggest a para- and/or autocrine function of the PGE₂-G/P2Y₆ pair. In line with this, P2Y receptors, including P2Y₆, are involved in inflammation, infection, and other (patho-)physiological conditions^{20,34}. As also shown by Zhang and co-workers, P2Y₆ is highly expressed in RAW264.7 cells and is possibly involved in macrophage-associated immune function³⁵. In addition, extracellular nucleotides are released in response to injury and inflammation to exert pro-inflammatory effects³⁶. Cell lysis results in an immediate release of nucleotides to reach a concentrations > 100 nM^{37,38}. This leads to stimulation of P2Y receptors to recruit macrophages. Similarly, PGE₂-G could act via P2Y₆ to regulate a fast and efficient recruitment of macrophages. We intensively addressed the possibility that PGE₂-G acts indirectly by release of nucleotides. As shown in Fig. 3f there is no evidence of ATP and ADP release after incubation with PGE₂-G since neither P2Y₁ nor P2Y₁₂ showed activity upon stimulation with PGE₂-G.

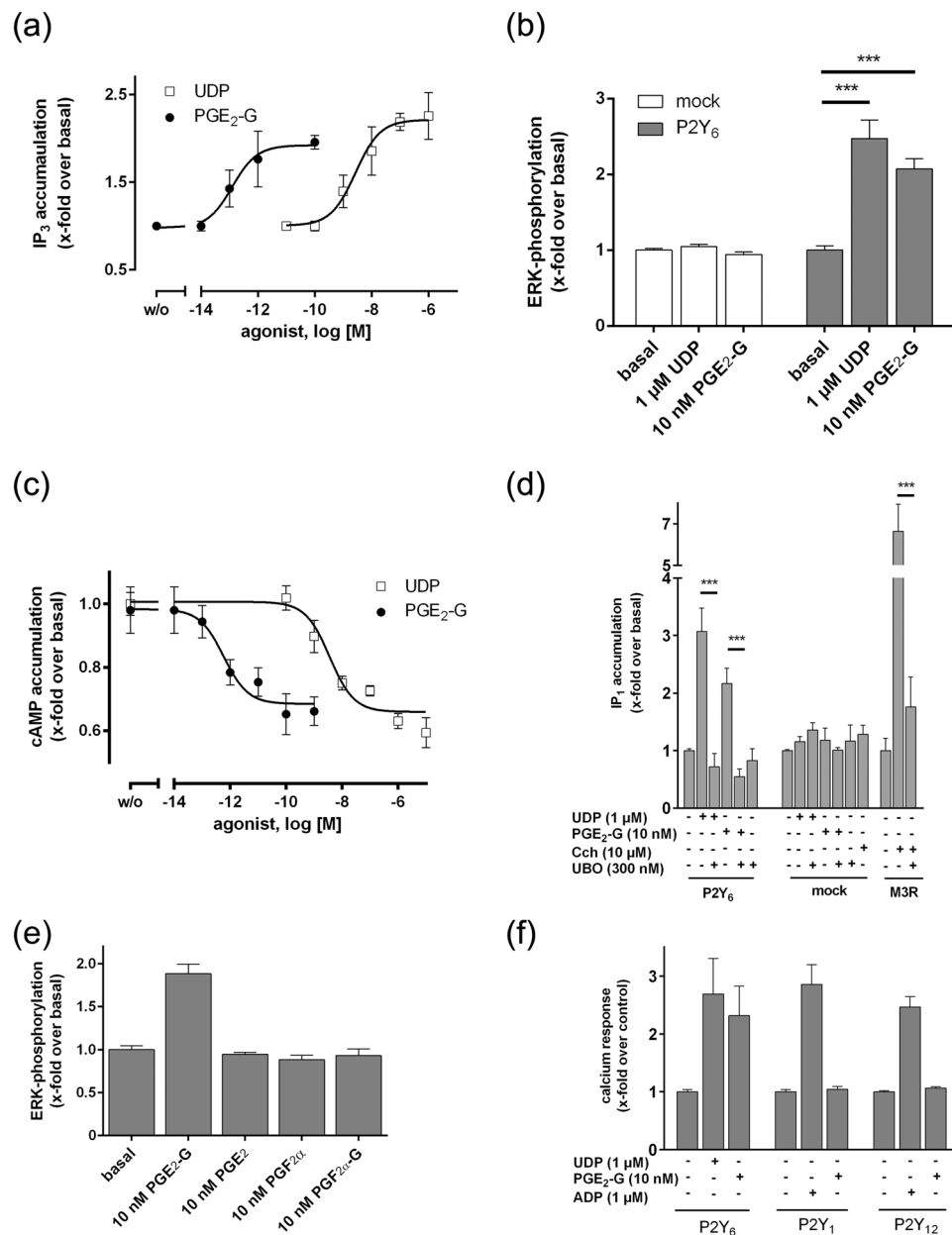


Figure 3. P2Y6 activated by UDP- and PGE₂-G couples to G_q- and G_{i/o} proteins. **(a)** In an IP₃ assay with P2RY6-transfected HEK293 cells, UDP and PGE₂-G revealed EC₅₀ values of 2.7 ± 0.1 nM and 0.2 ± 0.01 pM, respectively. **(b)** PGE₂-G and UDP induce ERK1/2 phosphorylation. Mock- and P2RY6-transfected HEK293 cells were treated with the indicated concentrations of UDP and PGE₂-G, and ERK phosphorylation was measured with the AlphaScreen® SureFire ERK 1/2 assay. **(c)** In a cAMP-inhibition assay HEK293 cells transfected with P2RY6 were incubated with various concentrations of PGE₂-G or UDP in the presence of 2.5 μM forskolin (see Methods). The EC₅₀ values of PGE₂-G and UDP were 0.6 ± 0.2 pM and 3.6 ± 0.3 nM, respectively. Basal cAMP levels before and after stimulation with forskolin were 2.3 ± 0.6 and 106 ± 7.3 nM/well, respectively. **(d)** HEK293 cells transfected with P2RY6 were incubated with UDP or PGE₂-G in the presence or absence of UBO and IP₁ accumulation assay was performed as described. As a control, the G_q protein-coupled muscarinic acetylcholine receptor (M3R) receptor stimulated with carbachol (Cch) was used. **(e)** HEK293 cells stably transfected with P2RY6 were incubated with indicated concentrations of prostaglandins and PG-Gs and ERK1/2 phosphorylation assay was performed as described under Methods. All concentrations were tested on empty vector- (mock-) transfected cells and showed no effect in the used second messenger assays. **(f)** The effect of PGE₂-G on intracellular Ca²⁺ release was determined in HEK293 cells transfected with P2RY1 or P2RY12 (see Methods). All data are means ± SEM of three independent experiments, each performed in triplicate. *p < 0.05, **p < 0.01, ***p < 0.001 (paired Student's t test).

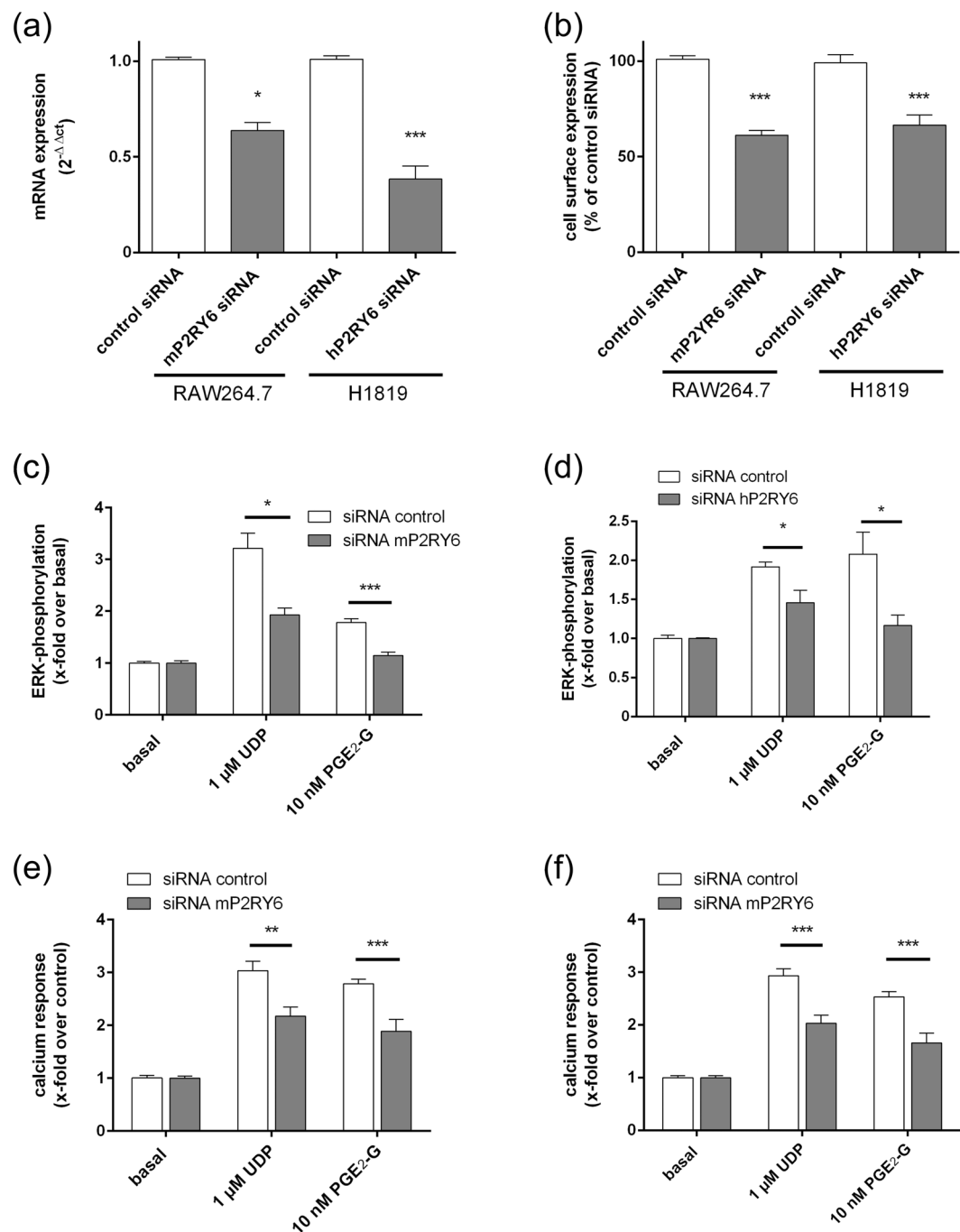


Figure 4. Knock-down of P2Y6 revealed decreased signal transduction of UDP and PGE₂-G. (a) and (b) RAW264.7 and H1819 were transfected with siRNA for mouse and human P2RY6, respectively. (a) mRNA expression levels of P2RY6 were determined (see Methods) and were normalized to $\beta 2$ -microglobulin (C_t were 14.6 ± 0.2 and 17.4 ± 0.1 for RAW264.7 and H1819, respectively). Values are given as mean of $2^{-\Delta\Delta C_t} \pm$ SEM and statistical analysis was performed according to ref. 58. (b) Protein expression levels of P2Y₆ were determined using a cell surface ELISA using an N-terminus-directed anti-P2Y₆ specific antibody (see Methods) and are given as OD at 492 nm. Data are given as means \pm SEM of three independent experiments performed in quadruplicates. (c–f) siRNA-transfected RAW264.7 (c,e) and H1819 (d,f) were incubated with the indicated concentrations of UDP and PGE₂-G, and ERK1/2 phosphorylation (c,d) and Ca²⁺ mobilization assays (e,f) were performed as described. All data are means \pm SEM of three independent experiments, each performed in triplicate. * $p < 0.05$, ** $p < 0.01$, *** $p < 0.001$ (paired Student's t test).

Further, the existence of mutations in P2Y₆ that discriminate between UDP and PGE₂-G excluded released UDP as cause of PGE₂-G-triggered P2Y₆ activation. It is rather evident that P2Y₆ integrates different chemical signals related to cell damage. There is growing evidence that GPCRs can have more than one endogenous agonist (agonist promiscuity). This concept is well established for chemokine receptors³⁹ but seems to occur also in other

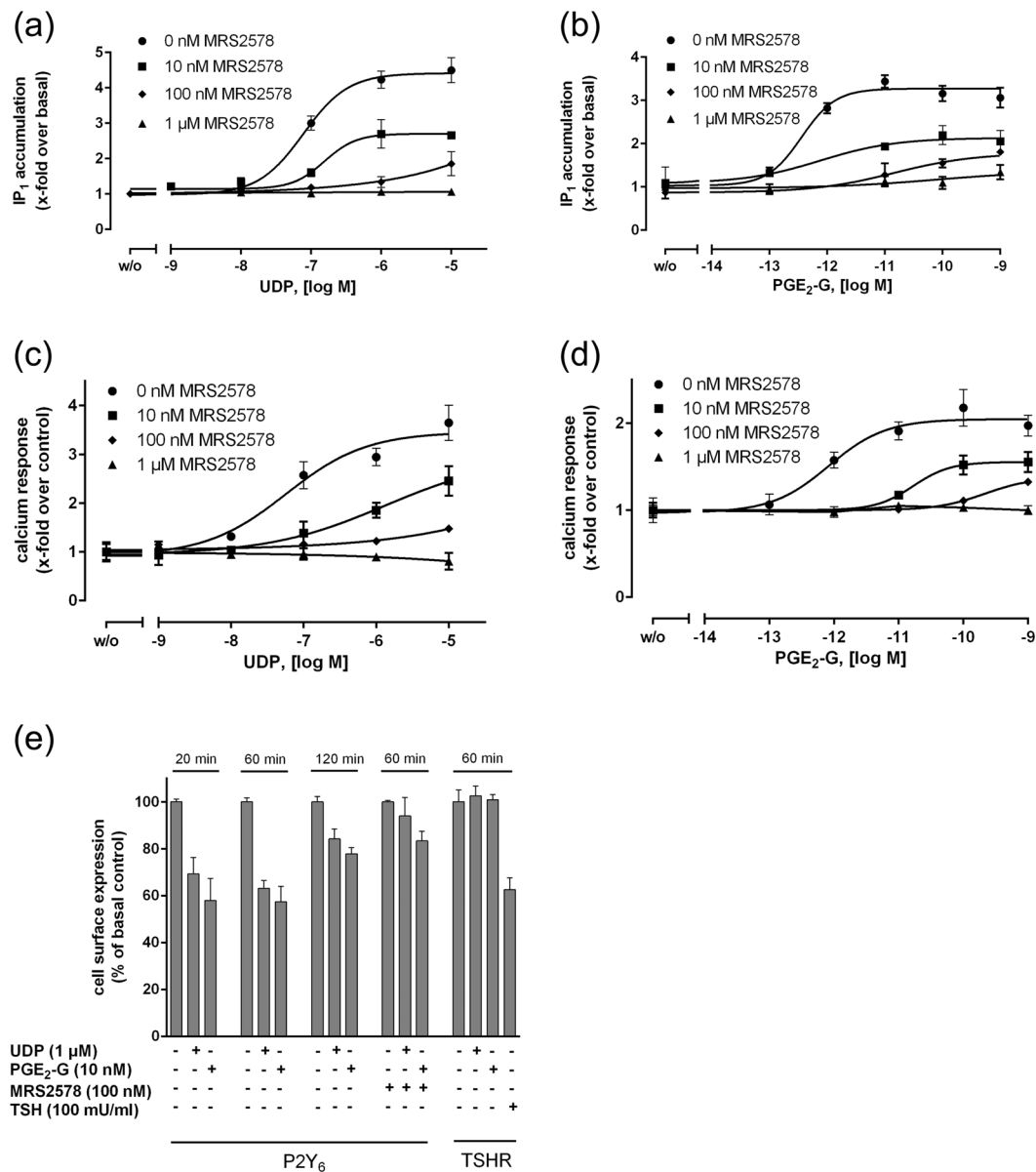


Figure 5. UDP- and PGE₂-G-induced signaling can be blocked by the P2Y₆ antagonist MRS2578. HEK293 cells were stably transfected with P2RY6, and the IP₁ accumulation assay and measurement of Ca²⁺ release was performed as described under *Methods*. Concentration-response curves of UDP (a,c) and PGE₂-G (b,d) were performed in the absence and presence of different concentrations of the antagonist MRS2578 in 1% DMSO. EC₅₀ values for UDP and PGE₂-G in IP₁ accumulation assay were 77.3 ± 3.4 nM and 0.3 ± 0.02 pM, respectively, and 57.1 ± 2.5 nM and 0.8 ± 0.08 pM in Ca²⁺ mobilization assay. Data are means \pm SEM of three independent experiments, each performed in triplicate. (e) HEK293 cells were transiently transfected with hP2RY6 and the HA-tagged human TSH receptor (TSHR) and the receptor expression levels were measured by cell surface ELISA (see *Methods*). Both, UDP and PGE₂-G induced a time-dependent internalization of the P2Y₆ whereas both compounds had no effect on the cell surface expression of the TSH receptor. The TSH receptor was stimulated with bovine TSH (100 mU/ml). The non-specific antibody binding to empty vector-transfected cells revealed an OD_{492nm} of 0.01 ± 0.002 . Data are given as mean \pm SEM of three independent experiments each performed in quadruplicates.

GPCRs. Previous studies on other P2Y receptors showed that, besides nucleotides, some paralogs and/or orthologues can be activated by aliphatic compounds like leukotrienes and phospholipids⁴⁰⁻⁴⁴.

MRS2578 reduced both, the efficacies and potencies of both agonists (see Fig. 5a-d) indicating that MRS2578 is an antagonist with mixed properties (competitive and non-competitive). This is compatible with both scenarios: a shared binding site but also different binding sites which is/are equally influenced by MRS2578. Since there is currently no competitive antagonist available for P2Y₆ the questions whether UDP and PGE₂-G share the binding pocket or bind at different sites is difficult to address experimentally. The potency difference of more than

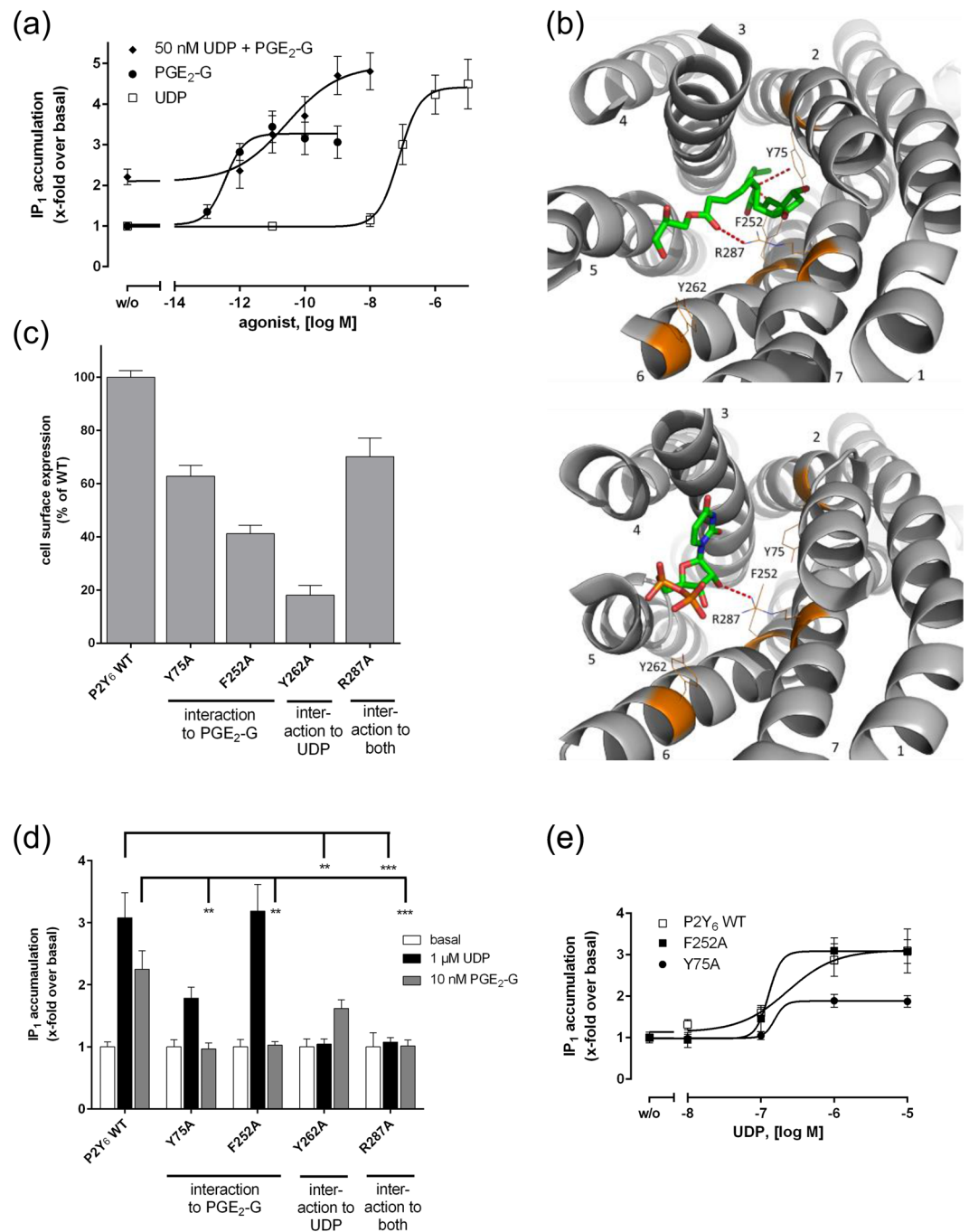


Figure 6. UDP and PGE₂-G have overlapping agonist binding sites. **(a)** Concentration-response curves of UDP and PGE₂-G alone and of PGE₂-G + 50 nM UDP on HEK293 cells transfected with P2RY6 were determined in IP₁ accumulation assays (see Methods). EC₅₀ values for UDP and PGE₂-G were 18.9 ± 2.3 nM and 0.3 ± 0.1 pM, respectively. **(b)** Extracellular view of the top scoring pose of PGE₂-G (green) docked in the comparative model of the P2Y₆ receptor (gray) (top) and top scoring pose of UDP (green) (bottom). Side chains of residues Y75, F252, Y262, and R287 are indicated as orange lines. Interactions captured in the majority of the top scoring poses are indicated as dashed red lines. Helices are numbered from N- to C-terminal. **(c)** Cell surface expression of mutant P2Y₆ receptors was determined as described. Optical density (OD) is given as percentage of P2Y₆ WT minus OD of mock-transfected cells. Data are given as means \pm SEM of three independent experiments performed in triplicate. **(d)** and **(e)** HEK293 cells were transfected with wildtype and mutant P2RY6 and IP₁ accumulation assays were performed as described. **(d)** Indicated concentrations of UDP and PGE₂-G were tested on mutant P2Y₆ receptors. **(e)** Indicated concentrations of UDP revealed EC₅₀ values of 15.4 ± 0.9 nM and 12.7 ± 2.1 nM for Y75A and F252A, respectively. All data are means \pm SEM of three independent experiments, each performed in triplicate. **p* < 0.05, ***p* < 0.01, ****p* < 0.001 (paired Student's *t* test).

4 orders of magnitude between both agonists already suggests different or additional agonist-receptor interaction sites within the P2Y₆ molecule.

If UDP and PGE₂-G share the agonist binding site one would expect receptor stimulation with an unchanged efficacy (E_{max} value) starting from increased basal IP levels (induced by the sub-maximum UDP concentration) as shown in Fig. 6a. EC₅₀ values for UDP (18.9 ± 2.3 nM) and PGE₂-G (0.3 ± 0.1 pM) showed the same ratio (~63,000) as observed in Ca²⁺ measurements in transfected HEK cells (~65,000, Fig. 2b). In the presence of sub-maximum UDP concentration (50 nM) the concentration-response curve of PGE₂-G was shifted to higher concentrations. The interpretation of this finding is difficult. It may reflect that UDP binds at a different site than PGE₂-G and allosterically influences the PGE₂-G binding site. Latter scenario would assume only one active receptor conformation induced by the two agonist binding sites. However, there is strong evidence that different agonists stabilize or induce different active conformations^{45,46}. In such scenario both agonists compete for the same binding site but stabilize or induce different active conformations. This would lead to a shift in the concentration-response curve in a competitive manner as seen in Fig. 6a. The fact that in most functional assays the E_{max} values of PGE₂-G are slightly lower compared to UDP (Figs 3a–c and 6a) may indicate different active conformations of P2Y₆ as seen for partial agonists⁴⁷.

To further address the questions whether UDP and PGE₂-G share the binding pocket or bind at different sites we generated a homology model of P2Y₆ and performed computer-aided ligand docking to predict the binding mode of both agonists. The predicted binding pockets of UDP and PGE₂-G revealed shared but also specific determinants for ligand orientation. Mutation of these residues to alanine and experimental testing of these mutants (Fig. 6d,e) supported our hypothesis that UDP and PGE₂-G most probably share interaction partners but additional determinants specific for each agonist contribute to the individual binding pockets.

In sum, we identified P2Y₆ as the GPCR for a COX-2-selective signal transduction pathway mediated by PGE₂-G. P2Y₆ integrates different chemical signals to a common intracellular response. Therefore, the indirect inactivation of the PGE₂-G/P2Y₆ signalling system by COX-2 inhibition most likely contributes to the pharmacological effects of nonsteroidal anti-inflammatory drugs such as ibuprofen and mefenamic acid⁴⁸.

Methods

Materials. If not stated otherwise, all chemicals were purchased from Sigma-Aldrich (Germany), and cell culture materials were provided by Life Technologies GmbH (Germany). FR900359 (UBO) was isolated and purified from the dried leaves of the evergreen plant *Ardisia crenata* using methanol (MeOH) extraction as described previously in detail²⁵.

Screening of orphan GPCRs with PGE₂-G. For screening orphan GPCRs as possible targets for PGE₂-G, the PathHunter[®] β-Arrestin assay (DiscoverX Co., USA) was used. It monitors the activation of a GPCR by utilizing an enzyme fragment complementation assay with β-galactosidase as the functional reporter. Briefly, the enzyme is split into two complementary portions expressed as fusion proteins in the cell. The enzyme acceptor is fused to β₂-arrestin, and the ProLink donor peptide is fused to the GPCR of interest. Upon GPCR stimulation, β₂-arrestin is recruited to the receptor, bringing the two fragments of β-galactosidase together. This generates an active enzyme that can convert a chemiluminescent substrate, generating a signal detectable on a standard microplate reader (see manufacturer's instructions). In total, 78 GPCRs, previously considered orphan and individually transfected into cells, were screened by DiscoverX (Supplementary Table S1). The percentage activity given in the results is calculated using the following formula: % activity = 100% × (mean RLU of test sample - mean RLU of vehicle control)/mean RLU of vehicle control).

Library construction and RNA sequencing. RAW264.7, H1819, A7r5, and HEK293 cells were purchased from ATCC[®]. A431 cells were a gift of Dr Stanley Cohen (Vanderbilt University, USA). Total RNA from RAW264.7, HEK293, A7r5, H1819, and A413 cells was isolated using TRI REAGENT[™] (Sigma-Aldrich) according to the manufacturer's instructions. RNA quantity was measured with a spectrometer (Nanodrop ND 1000), and RNA quality was analysed on the Agilent 2100 Bioanalyzer using the RNA 6000 Nano Chip (Agilent Technologies, USA). We only included RNA samples with an RIN value above 8. Indexed cDNA libraries were generated using TruSeq RNA Sample Preparation kits v2 (Illumina, USA) according to the manufacturer's protocol. The average library size was 300 bp as determined on the Agilent 2100 Bioanalyzer with DNA 1000 Chips.

The libraries were sequenced on the Illumina HiScanSQ Sequencing System (Interdisciplinary Centre for Clinical Research, Leipzig), generating on average 11.8 ± 1.5 million 101-bp raw paired-end reads per sample on one flow cell lane.

Gene quantification and differential expression analysis. After intensities call, raw reads were separated according to library indices allowing up to one mismatch in the index sequence, but requiring that all bases have a quality score above 15 (PHRED-scale). After assigning reads to samples, we used an in-house sequence analysing pipeline to trim the adapters and remove reads that were shorter than 60 bp or had more than five bases with a quality score below 15 (PHRED-scale). Reads were mapped to the reference genome of human (February 2009 GRCh37/hg19), mouse (July 2007 NCBI37/mm9), and rat (November 2004 rno4), respectively, using Tophat 2.0.6⁴⁹, which aligns reads using Bowtie2 v2.1.0. Reads that did not map uniquely to a genome position were excluded. Running a differential expression analysis across species boundaries is not a straightforward task, since the comparison would have to address issues like changes in gene structure, gene duplications, and deletions. Thus, we combined a differential expression analysis of the human cell lines with a general GPCR expression profile of human, mouse, and rat cell lines. To assess GPCR expression, we combined information from the HUGO gene nomenclature committee (HGNC)⁵⁰ and the EMBL-EBI InterPro database⁵¹ to retrieve a list of human GPCRs. Afterwards, the expression levels of these receptors in the respective cell lines, as well as

their orthologues from mouse and rat (retrieved via BioMart⁵² from Ensembl v82), were obtained as FPKM by using Cufflinks v2.1.1⁵³. A receptor with an FPKM >1 was considered to be expressed. For the differential expression analysis, the transcript level for each gene was obtained as read count by intersecting mapping results with gene annotations using BEDTools IntersectBed⁵⁴. Using the DESeq software package⁵⁵, differential expression of genes between the positive human cell line H1819 and the negative human cell lines HEK293 and A431 was examined. Differentially expressed genes with a p-value < 0.05 were considered as statistically significant.

Generation of receptor constructs. cDNA from H1819 cells was used to amplify and clone the P2RY6 and CNR2 coding sequences. They were double-tagged with an N-terminal HA epitope and a C-terminal FLAG epitope and, for transient transfection, introduced into the mammalian expression vector pcDps⁵⁶. All mutant constructs were generated by a PCR-based site-directed mutagenesis and fragment replacement strategy. For stable transfection, P2RY6 was sub-cloned into the pIRES-eGFP vector (CLONTECH Laboratories, USA). All constructs were verified by sequencing.

Cell culture and transfection. RAW264.7 cells were grown in DMEM supplemented with 10% FBS, A7r5 (rat fibroblast) cells in DMEM with 10% FBS, and A431 (human squamous carcinoma) cells in RPMI supplemented with 10% FBS. All cell lines were grown at 37 °C in a humidified 5% CO₂ incubator. For functional assays, receptor constructs were heterologously expressed in human embryonic kidney (HEK293) cells upon transient or stable transfection. Cells were grown in DMEM/F12 supplemented with 10% FBS, 100 units/ml penicillin, and 100 µg/ml streptomycin. For the cAMP-inhibition assay, ERK1/2 phosphorylation assay, and Ca²⁺ mobilization assay, cells were split into 96-well plates (2.0 × 10⁴ cells/well) and transfected with 250 ng vector construct using MACSfectin™ (Miltenyi Biotec, Germany) according to manufacturer's protocol. Empty vector (mock) served as the negative control. For siRNA experiments, cells were seeded in 6-well plates (4.0 × 10⁵ and 6.0 × 10⁵ cells/well for RAW264.7 and H1819, respectively). RAW264.7 and H1819 cells were transfected with 150 pMol of mP2RY6 siRNA and hP2RY6 siRNA (Santa Cruz Biotechnology, USA), respectively, using Viromer® Blue (Lipocalyx, Germany). As a negative control, control siRNA-A (Santa Cruz Biotechnology, USA) was used. FITC-labelled siRNA served as a transfection control.

To generate a cell line stably expressing P2Y₆, HEK293 cells were seeded in 6-well plates (7.5 × 10⁵ cells/well) and transfected with 3 µg vector using MACSfectin™ as transfection reagent according to the manufacturer's protocol. The pIRES-eGFP vector served as negative control. Stably transfected HEK293 cells were cultured in the presence of geneticin (500 µg/ml) for selection.

To estimate cell surface expression of heterologously expressed receptors carrying an N-terminal HA tag, an indirect cellular ELISA was used⁵⁷. To determine the endogenous cell surface expression of P2Y₆, the same ELISA procedure was performed with minor modifications. Briefly, after 4% paraformaldehyde fixation and blocking with 10% FBS, cells were incubated with the primary anti-P2Y₆ antibody (sc-15215; Santa Cruz Biotechnology, USA) in 1:1,000 dilution for 1 h. After washing with PBS, cells were incubated with peroxidase-conjugated secondary antibody anti-goat IgG (sc-2020, Santa Cruz Biotechnology, USA) in 1:5,000 dilutions.

Intracellular Ca²⁺ measurement. For fluorometric measurements of intracellular Ca²⁺ levels with the FlexStationII instrument (Molecular Devices), RAW264.7 and H1819 cells were seeded into 96-well plates (3.0 × 10⁴ cells/well) 24 h prior to assay. Ca²⁺ measurements with transiently transfected HEK293 cells were performed 48 h after transfection. Cells were loaded with 200 µl Calcium 5 reagent (Explorer Kit, Molecular Devices, USA) for 60 min at 37 °C, and the assay was performed as described¹¹. Agonists and inhibitors were solved in DMSO (100x) and diluted 1:20 in 96-well compound plates containing HBSS. 50 µl of compound solution were added to the assay plate resulting in final concentration of 1% DMSO. Fold-response was calculated by $RFU_{max} - RFU_{min}(\text{ligand}) / RFU_{max} - RFU_{min}(\text{vehicle})$. EC₅₀ values were calculated by using GraphPad Prism6 software (GraphPad, USA).

Measurement of ERK-phosphorylation. Cells were transferred to serum-free medium 2 h prior to assay. Ligands and controls (10 µl of 10× concentrates) were added to 90 µl medium and incubated for 5 min at 37 °C. The final concentration of DMSO was 0.2%. The reaction was stopped by aspiration of the medium and addition of 50 µl lysis buffer (PerkinElmer Life Sciences). To measure ERK1/2 phosphorylation, the AlphaScreen® SureFire ERK 1/2 assay kit (PerkinElmer Life Sciences) was used with the high sensitivity protocol. Phosphorylated ERK1/2 was measured in 384-well white OptiPlate microplates (PerkinElmer Life Sciences) with the Fusion AlphaScreen multilabel reader (PerkinElmer Life Sciences).

cAMP-inhibition assay. After transfection (72 h), cells were washed once with DMEM/F12 containing 1 mM 3-isobutyl-methyl-xanthine (IBMX) followed by incubation in the presence of the indicated compounds and forskolin (2.5 µM) for 15 min at 37 °C. The final concentration of DMSO was 1%. Cells were lysed in 25 µl lysis buffer (5 mM HEPES; 0.1% BSA; 0.3% Tween20; 1 mM IBMX; pH 7.4) and kept frozen at -20 °C until measurement. To measure cAMP concentration, the AlphaScreen cAMP assay kit (PerkinElmer Life Sciences) was used according to the manufacturer's protocol.

siRNA experiments and RT-qPCR. After transfection (24 h), cells were harvested and seeded overnight into 96-well plates (3.0 × 10⁴ H1819 cells/well and 2.5 × 10⁴ RAW264.7 cells/well) and 6-well plates (4.0 × 10⁵ cells/well) for functional assays and RNA isolation, respectively. Measurement of ERK1/2 phosphorylation and Ca²⁺ release was performed as described above. For analysis of receptor's mRNA expression after siRNA transfection (see above), RNA from cells was isolated using TRI REAGENT™ (Sigma-Aldrich) according to the manufacturer's instructions. For quantitative real-time PCR analysis (qPCR), 1 µg of total RNA was reverse-transcribed (Omniscript; Qiagen, Germany) using a mixture of oligo(dT) and random hexamer primers. qPCR was

performed by GoTaq[®] qPCR Master Mix (Promega Corporation, USA). cDNA from 25 ng total RNA and 0.2 μM forward and reverse primers was used. Oligonucleotide primers were: hP2RY6 5'-gaaccatgcttgggaagg-3' and 5'-ctgtgcccattgtccaccatc-3', mP2RY6 5'-ctctctgtcctggaccaac-3' and 5'-tgtcctgtccataactgcc-3'. The primers were designed to flank intron sequences. PCR was performed in an MX 3000 P instrument (Stratagene, USA) using the following protocol: 5 min 50 °C, 2 min 95 °C, and 40 cycles of 15 s 95 °C, 30 s 60 °C. To confirm the presence of a single amplicon, product melting curves were recorded. Threshold cycle (C_t) values were set within the exponential phase of the PCR. Data were normalized to human or mouse β2-microglobulin and ΔC_T values were used to calculate the relative expression levels. Gene regulation was statistically evaluated by the $2^{-\Delta\Delta C_t}$ method⁵⁸.

Measurement of intracellular inositol phosphates. To measure intracellular IP₃ the HitHunter[®] Inositol (1,4,5) Triphosphate Assay (DiscoverRx, USA) was used according to manufacturer's protocol. HEK293 cells stably transfected with hP2RY6 were seeded in a 384-well Black microtiter plate (15,000 cells/well) (Greiner Bio One, Germany) and incubated with indicated concentrations of UDP and PGE₂-G for 20 seconds. Reaction was stopped by adding 5 μl 0.2 N perchloric acid and measurement of IP₃ was performed with the Fusion AlphaScreen multilabel reader (PerkinElmer Life Sciences) according to manufacturer's protocol. To measure IP₁, HEK293 cells expressing wildtype and mutant P2Y₆ were seeded into 384-well plates (5,000 cells/well) 24 h prior assay. After aspiration of the medium, cells were incubated with indicated concentrations of agonists/antagonist for 1 h. IP₁ measurements using the IP-one HTFR[®] assay kit (Cisbio assays, USA) were performed according to manufacturer's protocol. The assays were performed with a final concentration of 1% DMSO.

Generation of a P2Y₆ comparative model and ligand docking. A comparative model of P2Y₆ was constructed using the protein structure prediction software package, ROSETTA version 3^{59–61}. The X-ray crystal structures of P2Y₁ and P2Y₁₂ (Protein Data Bank ID: 4xnw, 4ntj)^{62–64} were chosen as main templates based on high similarity to P2Y₆ (e-value of $3e^{-15}$ with a sequence coverage of 90%) according to a search using NCBI BLASTP on sequences from the Protein Data Bank (PDB). To increase conformational sampling, these templates were supplemented with rhodopsin (1u19, 2 × 72), β2-AR (2rh1, 3sn6), β1-AR (2vt4, 2y03), A2A (3eml, 3qak), CXCR4 (3odu), D3 (3pbl), H1 (3rze), M2 (3uon), S1P1 (3v2w), M3 (4daj), κ-OR (4djh), μ-OR (4dkl), N/OFQ (4ea3), δ-OR, (4ej4), 5HT-1B (4iar), and 5HT-2B (4ib4). An initial sequence alignment of twelve P2Y receptors was performed using clustalw⁶⁵ and a profile alignment of the GPCR templates was performed using MUSTANG⁶⁶. Finally, a profile-profile alignment was performed using clustalw and adjustments were made to ensure that all secondary structure elements were properly aligned while moving significant gaps to loop regions. To ease computational demands, the first 15 and last 12 residues of the P2Y₆ sequence were truncated.

After assigning coordinates to P2Y₆ residues from each template alignment using Rosetta's partial-thread application, RosettaCM⁶⁷ 'hybridizer' was used to combine segments across all templates in an iterative Monte Carlo approach to arrive at energetically favorable compositions. In brief, RosettaCM exchanges template fragments into a starting model to achieve energetically favorable hybrid template models. Any residues still lacking coordinates were modeled de novo using 3mer and 9mer fragments. Transmembrane segments, as predicted using OCTOPUS⁶⁸, were modeled within Rosetta's implicit membrane potential⁶⁹. In total, 32,000 all-atom models were generated. The resulting full sequence models were subjected to eight iterative cycles of side chain repacking and gradient minimization of ϕ , ψ , and χ angles within the membrane potential. P2Y₆, P2Y₁, and P2Y₁₂ share a conserved disulfide bond between the N-terminal C18 and C273 in extracellular loop 3⁷⁰. Residue pair constraints were introduced between these residues as well as C99 and C177. The top 50% of all relaxed generated models by pose score were clustered by RMSD using BCL::Cluster⁷¹ with a node similarity of 4 Å. The top scoring models from the three largest clusters were collected along with the top scoring models overall. Following visual inspection, a final set of 14 models were selected for docking.

Ligand docking into the comparative model of P2Y₆ with UDP and PGE₂-G was performed with Rosetta Ligand^{72, 73}. One hundred conformations of PGE₂-G and thirteen conformations of UDP were generated with BCL::Conf⁷⁴. This application builds small molecule conformations from active substructures seen in experimentally elucidated structures. For both ligands, a starting position was selected based on the average position of ligands present in all GPCR templates. The docking protocol included a low resolution (centroid mode) phase consisting of 50 cycles of 4 Å translation search and 500 cycles of 360° rotation search and a high resolution phase consisting of six cycles of side chain refinement. This phase finds an energetically favorable pose by combining minor ligand conformational flexibility with side chain refinement simultaneously. For each ligand, 12,000 poses were generated in the first round of docking. The top 50 models by interface_delta score were collected for each ligand and a second round of docking was performed beginning with each selected pose. For the second round of docking, the translation and rotation searchers were reduced to 2 Å and 180° respectively. A third focused round was performed from the same selection scheme with 1 Å and 90° search. All ligand poses generated in the third round of focused docking were clustered using BCL::Cluster and a final ensemble of 10 models for each ligand were selected based on cluster size and interface_delta. Because the docking runs did not converge on a single conformation for either ligand, all poses within the top scoring ensembles were considered for contact analysis. For each ensemble pose, the change in free energy with and without ligands bound to P2Y₆ was calculated for each residue in the receptor. Residues with the greatest difference in predicted energy across the majority of ensemble models are suggested to be important for ligand interaction (Supplementary figure S1).

References

- Smith, W. L. Prostanoid biosynthesis and mechanisms of action. *The American journal of physiology* **263**, F181–91 (1992).
- Kozak, K. R., Rowlinson, S. W. & Marnett, L. J. Oxygenation of the endocannabinoid, 2-arachidonylglycerol, to glyceryl prostaglandins by cyclooxygenase-2. *The Journal of biological chemistry* **275**, 33744–33749 (2000).

3. Kozak, K. R. *et al.* Metabolism of the endocannabinoids, 2-arachidonoylglycerol and anandamide, into prostaglandin, thromboxane, and prostacyclin glycerol esters and ethanolamides. *The Journal of biological chemistry* **277**, 44877–44885 (2002).
4. Kozak, K. R. *et al.* Metabolism of prostaglandin glycerol esters and prostaglandin ethanolamides *in vitro* and *in vivo*. *The Journal of biological chemistry* **276**, 36993–36998 (2001).
5. Alhouayek, M., Masquelier, J., Cani, P. D., Lambert, D. M. & Muccioli, G. G. Implication of the anti-inflammatory bioactive lipid prostaglandin D2-glycerol ester in the control of macrophage activation and inflammation by ABHD6. *Proceedings of the National Academy of Sciences of the United States of America* **110**, 17558–17563 (2013).
6. Kingsley, P. J., Rouzer, C. A., Saleh, S. & Marnett, L. J. Simultaneous analysis of prostaglandin glyceryl esters and prostaglandins by electrospray tandem mass spectrometry. *Analytical biochemistry* **343**, 203–211 (2005).
7. Rouzer, C. A. & Marnett, L. J. Glycerylprostaglandin synthesis by resident peritoneal macrophages in response to a zymosan stimulus. *The Journal of biological chemistry* **280**, 26690–26700 (2005).
8. Rouzer, C. A. *et al.* Zymosan-induced glycerylprostaglandin and prostaglandin synthesis in resident peritoneal macrophages: roles of cyclo-oxygenase-1 and -2. *The Biochemical journal* **399**, 91–99 (2006).
9. Hu, S. S.-J., Bradshaw, H. B., Chen, J. S.-C., Tan, B. & Walker, J. M. Prostaglandin E2 glycerol ester, an endogenous COX-2 metabolite of 2-arachidonoylglycerol, induces hyperalgesia and modulates NF κ B activity. *British journal of pharmacology* **153**, 1538–1549 (2008).
10. Sang, N., Zhang, J. & Chen, C. COX-2 oxidative metabolite of endocannabinoid 2-AG enhances excitatory glutamatergic synaptic transmission and induces neurotoxicity. *Journal of neurochemistry* **102**, 1966–1977 (2007).
11. Nirodi, C. S., Crews, B. C., Kozak, K. R., Morrow, J. D. & Marnett, L. J. The glyceryl ester of prostaglandin E2 mobilizes calcium and activates signal transduction in RAW264.7 cells. *Proceedings of the National Academy of Sciences of the United States of America* **101**, 1840–1845 (2004).
12. Richie-Jannetta, R. *et al.* Structural determinants for calcium mobilization by prostaglandin E2 and prostaglandin F2 α glyceryl esters in RAW 264.7 cells and H1819 cells. *Prostaglandins & other lipid mediators* **92**, 19–24 (2010).
13. Matias, I. *et al.* Prostaglandin ethanolamides (prostamides): *in vitro* pharmacology and metabolism. *The Journal of pharmacology and experimental therapeutics* **309**, 745–757 (2004).
14. Hannedouche, S. *et al.* Oxysterols direct immune cell migration via EBI2. *Nature* **475**, 524–527 (2011).
15. Liu, C. *et al.* Oxysterols direct B-cell migration through EBI2. *Nature* **475**, 519–523 (2011).
16. Rosenkilde, M. M. *et al.* Molecular pharmacological phenotyping of EBI2. An orphan seven-transmembrane receptor with constitutive activity. *The Journal of biological chemistry* **281**, 13199–13208 (2006).
17. Xiong, N., Fu, Y., Hu, S., Xia, M. & Yang, J. CCR10 and its ligands in regulation of epithelial immunity and diseases. *Protein & cell* **3**, 571–580 (2012).
18. Horiguchi, K. *et al.* Proton receptor GPR68 expression in dendritic-cell-like S100 β -positive cells of rat anterior pituitary gland: GPR68 induces interleukin-6 gene expression in extracellular acidification. *Cell and tissue research* **358**, 515–525 (2014).
19. Cohen, L. J. *et al.* Functional metagenomic discovery of bacterial effectors in the human microbiome and isolation of commensamide, a GPCR G2A/132 agonist. *Proceedings of the National Academy of Sciences of the United States of America* **112**, E4825–34 (2015).
20. Abbracchio, M. P. *et al.* International Union of Pharmacology LVIII: update on the P2Y G protein-coupled nucleotide receptors: from molecular mechanisms and pathophysiology to therapy. *Pharmacological reviews* **58**, 281–341 (2006).
21. Communi, D., Parmentier, M. & Boeynaems, J. M. Cloning, functional expression and tissue distribution of the human P2Y6 receptor. *Biochemical and biophysical research communications* **222**, 303–308 (1996).
22. Filippov, A. K., Webb, T. E., Barnard, E. A. & Brown, D. A. Dual coupling of heterologously-expressed rat P2Y6 nucleotide receptors to N-type Ca $^{2+}$ and M-type K $^{+}$ currents in rat sympathetic neurones. *British journal of pharmacology* **126**, 1009–1017 (1999).
23. Sugiura, T., Kondo, S., Nakane, S. & Waku, K. [2-Arachidonoylglycerol: an endogenous cannabinoid receptor agonist]. *Tanpakushitsu kakusan koso. Protein, nucleic acid, enzyme* **44**, 1104–1110 (1999).
24. Ko, H. *et al.* Synthesis and potency of novel uracil nucleotides and derivatives as P2Y2 and P2Y6 receptor agonists. *Bioorganic & medicinal chemistry* **16**, 6319–6332 (2008).
25. Schrage, R. *et al.* The experimental power of FR900359 to study Gq-regulated biological processes. *Nature communications* **6**, 10156 (2015).
26. Mamedova, L. K., Joshi, B. V., Gao, Z.-G., Kügelgen, I. von & Jacobson, K. A. Diisothiocyanate derivatives as potent, insurmountable antagonists of P2Y6 nucleotide receptors. *Biochemical pharmacology* **67**, 1763–1770 (2004).
27. Civelli, O. *et al.* G protein-coupled receptor deorphanizations. *Annual review of pharmacology and toxicology* **53**, 127–146 (2013).
28. Bar, I. *et al.* Knockout mice reveal a role for P2Y6 receptor in macrophages, endothelial cells, and vascular smooth muscle cells. *Molecular pharmacology* **74**, 777–784 (2008).
29. Garcia, R. A. *et al.* P2Y6 receptor potentiates pro-inflammatory responses in macrophages and exhibits differential roles in atherosclerotic lesion development. *PloS one* **9**, e111385 (2014).
30. Giannattasio, G. *et al.* The purinergic G protein-coupled receptor 6 inhibits effector T cell activation in allergic pulmonary inflammation. *Journal of immunology (Baltimore, Md.: 1950)* **187**, 1486–1495 (2011).
31. Stachon, P. *et al.* P2Y6 deficiency limits vascular inflammation and atherosclerosis in mice. *Arteriosclerosis, thrombosis, and vascular biology* **34**, 2237–2245 (2014).
32. Ghilardi, J. R., Svensson, C. I., Rogers, S. D., Yaksh, T. L. & Mantyh, P. W. Constitutive spinal cyclooxygenase-2 participates in the initiation of tissue injury-induced hyperalgesia. *The Journal of neuroscience: the official journal of the Society for Neuroscience* **24**, 2727–2732 (2004).
33. Woodward, D. F. *et al.* The pharmacology and therapeutic relevance of endocannabinoid derived cyclo-oxygenase (COX)-2 products. *Pharmacology & therapeutics* **120**, 71–80 (2008).
34. Boeynaems, J.-M., Communi, D., Gonzalez, N. S. & Robaye, B. Overview of the P2 receptors. *Seminars in thrombosis and hemostasis* **31**, 139–149 (2005).
35. Zhang, Z. *et al.* P2Y(6) agonist uridine 5'-diphosphate promotes host defense against bacterial infection via monocyte chemoattractant protein-1-mediated monocytes/macrophages recruitment. *Journal of immunology (Baltimore, Md.: 1950)* **186**, 5376–5387 (2011).
36. Boeynaems, J.-M. & Communi, D. Modulation of inflammation by extracellular nucleotides. *The Journal of investigative dermatology* **126**, 943–944 (2006).
37. Communi, D., Janssens, R., Suarez-Huerta, N., Robaye, B. & Boeynaems, J. M. Advances in signalling by extracellular nucleotides. the role and transduction mechanisms of P2Y receptors. *Cellular signalling* **12**, 351–360 (2000).
38. Lazarowski, E. R., Boucher, R. C. & Harden, T. K. Mechanisms of release of nucleotides and integration of their action as P2X- and P2Y-receptor activating molecules. *Molecular pharmacology* **64**, 785–795 (2003).
39. Southan, C. *et al.* The IUPHAR/BPS Guide to PHARMACOLOGY in 2016: towards curated quantitative interactions between 1300 protein targets and 6000 ligands. *Nucleic acids research* **44**, D1054–68 (2016).
40. Paruchuri, S. *et al.* Leukotriene E4-induced pulmonary inflammation is mediated by the P2Y12 receptor. *The Journal of experimental medicine* **206**, 2543–2555 (2009).
41. Pugliese, A. M. *et al.* Functional characterization of two isoforms of the P2Y-like receptor GPR17: [35S]GTP γ S binding and electrophysiological studies in 1321N1 cells. *American journal of physiology. Cell physiology* **297**, C1028–40 (2009).

42. Ritscher, L. *et al.* The ligand specificity of the G-protein-coupled receptor GPR34. *The Biochemical journal* **443**, 841–850 (2012).
43. Schmidt, P. *et al.* Identification of determinants required for agonistic and inverse agonistic ligand properties at the ADP receptor P2Y₁₂. *Molecular pharmacology* **83**, 256–266 (2013).
44. Schöneberg, T. *et al.* Structural and functional evolution of the P2Y₁₂-like receptor group. *Purinergic signalling* **3**, 255–268 (2007).
45. Gudermann, T., Kalkbrenner, F. & Schultz, G. Diversity and selectivity of receptor-G protein interaction. *Annual review of pharmacology and toxicology* **36**, 429–459 (1996).
46. Luttrell, L. M., Maudsley, S. & Bohn, L. M. Fulfilling the Promise of “Biased” G Protein-Coupled Receptor Agonism. *Molecular pharmacology* **88**, 579–588 (2015).
47. Yao, X. *et al.* Coupling ligand structure to specific conformational switches in the beta₂-adrenoceptor. *Nature chemical biology* **2**, 417–422 (2006).
48. Prusakiewicz, J. J., Duggan, K. C., Rouzer, C. A. & Marnett, L. J. Differential sensitivity and mechanism of inhibition of COX-2 oxygenation of arachidonic acid and 2-arachidonoylglycerol by ibuprofen and mefenamic acid. *Biochemistry* **48**, 7353–7355 (2009).
49. Langmead, B., Trapnell, C., Pop, M. & Salzberg, S. L. Ultrafast and memory-efficient alignment of short DNA sequences to the human genome. *Genome biology* **10**, R25 (2009).
50. Gray, K. A., Yates, B., Seal, R. L., Wright, M. W. & Bruford, E. A. Genenames.org: the HGNC resources in 2015. *Nucleic acids research* **43**, D1079–85 (2015).
51. Hunter, S. *et al.* InterPro: the integrative protein signature database. *Nucleic acids research* **37**, D211–5 (2009).
52. Smedley, D. *et al.* The BioMart community portal: an innovative alternative to large, centralized data repositories. *Nucleic acids research* **43**, W589–98 (2015).
53. Trapnell, C. *et al.* Differential gene and transcript expression analysis of RNA-seq experiments with TopHat and Cufflinks. *Nature protocols* **7**, 562–578 (2012).
54. Quinlan, A. R. & Hall, I. M. BEDTools: a flexible suite of utilities for comparing genomic features. *Bioinformatics (Oxford, England)* **26**, 841–842 (2010).
55. Anders, S. & Huber, W. Differential expression analysis for sequence count data. *Genome biology* **11**, R106 (2010).
56. Sangkuhl, K., Schulz, A., Schultz, G. & Schöneberg, T. Structural requirements for mutational lutropin/choriogonadotropin receptor activation. *The Journal of biological chemistry* **277**, 47748–47755 (2002).
57. Schöneberg, T. *et al.* V2 vasopressin receptor dysfunction in nephrogenic diabetes insipidus caused by different molecular mechanisms. *Human mutation* **12**, 196–205 (1998).
58. Livak, K. J. & Schmittgen, T. D. Analysis of relative gene expression data using real-time quantitative PCR and the 2^{(-Delta Delta C(T))} Method. *Methods (San Diego, Calif)* **25**, 402–408 (2001).
59. Bender, B. J. *et al.* Protocols for Molecular Modeling with Rosetta3 and RosettaScripts. *Biochemistry* **55**, 4748–4763 (2016).
60. Leaver-Fay, A. *et al.* ROSETTA3: an object-oriented software suite for the simulation and design of macromolecules. *Methods in enzymology* **487**, 545–574 (2011).
61. Rohl, C. A., Strauss, C. E., Misura, K. M. & Baker, D. In *Numerical computer methods* edited by Brand, L. & Johnson, M. L. pp. 66–93 (Academic, Amsterdam, London, 1992).
62. Zhang, D. *et al.* Two disparate ligand-binding sites in the human P2Y₁ receptor. *Nature* **520**, 317–321 (2015).
63. Zhang, J. *et al.* Agonist-bound structure of the human P2Y₁₂ receptor. *Nature* **509**, 119–122 (2014).
64. Zhang, K. *et al.* Structure of the human P2Y₁₂ receptor in complex with an antithrombotic drug. *Nature* **509**, 115–118 (2014).
65. Larkin, M. A. *et al.* Clustal W and Clustal X version 2.0. *Bioinformatics (Oxford, England)* **23**, 2947–2948 (2007).
66. Konagurthu, A. S., Whisstock, J. C., Stuckey, P. J. & Lesk, A. M. MUSTANG: a multiple structural alignment algorithm. *Proteins* **64**, 559–574 (2006).
67. Song, Y. *et al.* High-resolution comparative modeling with RosettaCM. *Structure (London, England: 1993)* **21**, 1735–1742 (2013).
68. Viklund, H. & Elofsson, A. OCTOPUS: improving topology prediction by two-track ANN-based preference scores and an extended topological grammar. *Bioinformatics (Oxford, England)* **24**, 1662–1668 (2008).
69. Yarov-Yarovoy, V., Schonbrun, J. & Baker, D. Multipass membrane protein structure prediction using Rosetta. *Proteins* **62**, 1010–1025 (2006).
70. Deflorian, F. & Jacobson, K. A. Comparison of three GPCR structural templates for modeling of the P2Y₁₂ nucleotide receptor. *Journal of computer-aided molecular design* **25**, 329–338 (2011).
71. Alexander, N., Woetzel, N. & Meiler, J. bcl::Cluster. A method for clustering biological molecules coupled with visualization in the Pymol Molecular Graphics System. *IEEE... International Conference on Computational Advances in Bio and Medical Sciences: [proceedings]. IEEE International Conference on Computational Advances in Bio and Medical Sciences* **2011**, 13–18 (2011).
72. Meiler, J. & Baker, D. RosettaLigand: protein-small molecule docking with full side-chain flexibility. *Proteins* **65**, 538–548 (2006).
73. Davis, I. W. & Baker, D. RosettaLigand docking with full ligand and receptor flexibility. *Journal of molecular biology* **385**, 381–392 (2009).
74. Kothiwale, S., Mendenhall, J. L. & Meiler, J. BCL::Conf: small molecule conformational sampling using a knowledge based rotamer library. *Journal of cheminformatics* **7**, 47 (2015).

Acknowledgements

We thank Anne Butthof for library preparation and Katja Ettig for excellent technical assistance. We are grateful to Dr. P. Jeffrey Conn and Prof. A.G. Beck-Sickinger for use of the FlexStation. This work was supported by the German Research Foundation (SCHO624/9-1) and GM15431 (Vanderbilt University). Anne Zimmermann was supported by the MD program of the Medical Faculty, University Leipzig.

Author Contributions

A.B., A.Z., B.C.C. performed the experiments. G.S., J.M. performed the generation of a receptor model and ligand docking. G.K., E.K. prepared UBO. V.L. performed the RNA-Seq studies and analysis. A.B., A.Z., T.S. analyzed the data. A.B., L.J.M., T.S. designed the study and wrote the paper with contributions from all authors.

Additional Information

Supplementary information accompanies this paper at doi:10.1038/s41598-017-02414-8

Competing Interests: The authors declare that they have no competing interests.

Publisher's note: Springer Nature remains neutral with regard to jurisdictional claims in published maps and institutional affiliations.



Open Access This article is licensed under a Creative Commons Attribution 4.0 International License, which permits use, sharing, adaptation, distribution and reproduction in any medium or format, as long as you give appropriate credit to the original author(s) and the source, provide a link to the Creative Commons license, and indicate if changes were made. The images or other third party material in this article are included in the article's Creative Commons license, unless indicated otherwise in a credit line to the material. If material is not included in the article's Creative Commons license and your intended use is not permitted by statutory regulation or exceeds the permitted use, you will need to obtain permission directly from the copyright holder. To view a copy of this license, visit <http://creativecommons.org/licenses/by/4.0/>.

© The Author(s) 2017